Applied Surface Science 282 (2013) 782–788

Contents lists available at SciVerse ScienceDirect

Applied Surface Science

journal homepage: www.elsevier.com/locate/apsusc

Eu-doped ZnO nanowire arrays grown by electrodeposition

O. Lupan[a,b,c,d,*], T. Pauporté[a,*], B. Viana[b], P. Aschehoug[b], M. Ahmadi[c], B. Roldan Cuenya[c], Y. Rudzevich[c], Y. Lin[c], L. Chow[c]

[a] Laboratoire d'Electrochimie, Chimie des Interfaces et Modélisation pour l'Energie (LECIME), UMR-7575, ENSCP-Chimie Paristech, 11 rue Pierre et Marie Curie, 75231 Paris cedex 05, France
[b] Laboratoire de Chimie de la Matière Condensée de Paris, UMR 7574, ENSCP, 11 rue P. et M. Curie, 75231 Paris cedex 05, France
[c] Department of Physics, University of Central Florida, Orlando, FL 32816, USA
[d] Department of Microelectronics and Semiconductor Devices, Technical University of Moldova, 168 Stefan cel Mare Blvd., Chisinau MD-2004, Republic of Moldova

ARTICLE INFO

Article history:
Received 25 March 2013
Received in revised form 9 June 2013
Accepted 10 June 2013
Available online 15 June 2013

Keywords:
ZnO
Europium doping
Nanowires
Electrodeposition
Photoluminescence

ABSTRACT

The preparation of efficient light emitting diodes requires active optical layers working at low voltage for light emission. Trivalent lanthanide doped wide-bandgap semiconducting oxide nanostructures are promising active materials in opto-electronic devices. In this work we report on the electrochemical deposition (ECD) of Eu-doped ZnO (ZnO:Eu) nanowire arrays on glass substrates coated with F-doped polycrystalline SnO_2. The structural, chemical and optical properties of ZnO:Eu nanowires have been systematically characterized by X-ray diffraction, transmission electron microscopy, Raman spectroscopy, X-ray photoelectron spectroscopy, secondary ion mass spectrometry, and photoluminescence. XRD results suggest the substitution of Zn^{2+} by Eu ions in the crystalline lattice. High-resolution TEM and associated electron diffraction studies indicate an interplanar spacing of 0.52 nm which corresponds to the (0 0 0 1) crystal plane of the hexagonal ZnO, and a growth along the *c*-direction. The ZnO:Eu nanowires have a single crystal structure, without noticeable defects. According to EDX, SIMS and XPS studies, cationic Eu species are detected in these samples showing the incorporation of Eu into the ZnO matrix. The oxidation states of europium ions in the nanowires are determined as +3 (74%) and +2 (26%). Photoluminescence studies demonstrated red emission from the Eu-doped ZnO nanowire arrays. When Eu was incorporated during the nanowire growth, the sharp $^5D_0$–$^7F_2$ transition of the Eu^{3+} ion at around 612 nm was observed. These results suggest that Eu doped ZnO nanowires could pave the way for efficient, multispectral LEDs and optical devices.

1. Introduction

For high-performance light emitting devices, efficient emissions are required by applying low voltages to an optically active layer [1–4]. Trivalent lanthanides doped semiconducting oxide nanostructures are one of the most promising nanomaterials for an active layer due to their stable intra-4f shell transitions in their ions [5]. In this context, zinc oxide (ZnO) possesses a great potential as a host material for europium-doped semiconductor [6–11] because it has a wide band gap of about 3.36 eV, a large exciton binding energy of 60 meV [7] and native defects [8,9]. The preparation and characterizations of the optical properties of ZnO doped with Eu^{3+} ions have been studied previously [10–21]. Pauporté et al. have developed an electrochemical precipitation technique for the preparation of the ZnO/Eu mixed layers [11,12]. In the Eu^{3+}-doped ZnO rod-shaped columns surrounded by a Eu/ZnO mixed basal layer, the energy transfer from ZnO to Eu^{3+} under UV light excitation was demonstrated [11]. The electrochemical preparation was explained in the light of a thermochemical study of the Eu–Cl–H_2O system [12]. Other growth routes from solution include spray pyrolysis [22,23], sol–gel [24] and coprecipitation [25]. Wang et al. [18] reported on defect-mediated energy transfer in red-light-emitting Eu-doped ZnO nanowire arrays prepared by a vapor transport method. Pan et al. [19] studied the growth by chemical vapor deposition of single crystal ZnO nanowires diffused with europium (Eu) from a solid source at 900 °C for 1 h. Chen et al. [17] reported on Eu-treated ZnO nanowires and found that the Eu^{3+} ions were in the Eu_2O_3-like state located at the surface of ZnO nanowire and red emission was detected. Yang et al. [15] showed Eu-doped ZnO nanowires prepared by high-temperature and high-pressure pulsed-laser deposition and emission near 611 nm and 755 nm.

* Corresponding authors at: Laboratoire d'Electrochimie, Chimie des Interfaces et Modélisation pour l'Energie (LECIME), UMR-7575, ENSCP-Chimie Paristech, 11 rue Pierre et Marie Curie, 75231 Paris cedex 05, France. Tel.: +33 1 55 42 63 83; fax: +33 1 44 27 67 50.
E-mail addresses: oleg-lupan@chimie-paristech.fr (O. Lupan), thierry-pauporte@chimie-paristech.fr (T. Pauporté).

0169-4332/$ – see front matter © 2013 Elsevier B.V. All rights reserved.
http://dx.doi.org/10.1016/j.apsusc.2013.06.053

However, for various cost-effective optoelectronic applications it is important to use a low-cost technique for tuning the emission wavelength of the nanowires for fabrication of ZnO based devices [1,3,4,26]. Although, it has been demonstrated that the bandgap of ZnO films can be tuned by the addition of dopants, several issues have to be clarified, such as the possibility of doping nanowires at controlled level through a cost-effective and efficient electrochemical process.

To the best of our knowledge, the direct electrodeposition of Eu-doped ZnO nanowire arrays with rather high aspect ratio has not been reported. In this paper we present the electrochemical deposition (ECD) technique for the direct synthesis of Eu-doped ZnO nanowire arrays. The composition, crystallographic structure and luminescence properties of the nanostructures are investigated and discussed.

2. Experimental

The nanowire arrays were electrodeposited in a three-electrode electrochemical cell using an aqueous solution containing 0.2 mmol L^{-1} $ZnCl_2$, 0.1 mol L^{-1} KCl as supporting electrolyte and continuous oxygen bubbling in a bath solution [4,27,28]. Three different concentrations of $EuCl_3$ (99.9% $EuCl_3$ $4H_2O$, Alfa Aesar) have been tested in the present work, 0 μmol L^{-1}, 1.0 μmol L^{-1} and 2.5 μmol L^{-1}, giving rise to the samples noted as #1, #2 and #3, respectively. Glass coated with F-doped polycrystalline SnO_2 (FTO) (resistance of 10 Ω/sq) was used as substrate. The substrates were cleaned in acetone, then ethanol (95%) for 6 min each in the ultrasonic bath, then in HNO_3 (45%) for 2 min, followed by rinsing with deionized water (18.2 MΩ cm) flow. Afterwards, the FTO substrates were mounted as a working electrode. Electrodeposition was performed potentiostatically at −1.0 V versus the SCE reference electrode using an Autolab PGSTAT30 potentiostat/galvanostat and with working electrode rotated at a constant speed of ω = 300 rotations/min. The deposition time was 9000 s and the bath temperature was fixed at 90 °C. After deposition, the layers were thoroughly rinsed with deionized water and dried in air to remove chloride salts and un-reacted products from the surface. Afterwards, it was subjected to thermal annealing in air at 300 °C for 1.0 h.

Scanning electron microscopy (SEM) images were obtained by using an Ultra 55 Zeiss FEG at an acceleration voltage of 15 kV. Quantitative elemental analyses (EDX) were realized with a Bruker Li-drift silicon detector. For structural characterization, a high-resolution X-ray diffractometer Siemens D5000 operated with 40 kV and 45 mA using the $CuK_{\alpha 1}$ radiation with λ = 1.5406 Å and a rotating sample holder were used. A TEM sample #3 was prepared by direct transfer of nanowires to carbon holey grid. Transmission electron microscopy (TEM) and selected area electron diffraction (SAED) measurements were performed on a FEI Tecnai F30 TEM transmission electron microscope operated at an accelerating voltage of 300 kV. Secondary ion mass spectrometry (SIMS) was used for the analysis of the Eu content in our samples due to its sensitivity and depth resolution [29]. SIMS studies were carried out with a Physical Electronics ADEPT 1010 quadrupole analyzer with a 3 keV Cs^+ primary beam at 60° from normal. The typical primary beam current was 25 nA. The primary beam was scanned over a 300 μm by 300 μm area, with detection of negative secondary ions from an area of 100 μm by 100 μm at the center of the scanned area.

X-ray photoelectron spectroscopy (XPS) measurements were performed in a modular ultrahigh vacuum (UHV) system (SPECS GmbH) specially designed for the preparation and characterization of nanoscale materials. The analysis chamber was equipped with a hemispherical electron energy analyzer (Phoibos 100) and dual-anode (Al-Kα, 1486.6 eV and Ag-Lα, 2984.4 eV) monochromatic X-ray source (XR50, SPECS GmbH) for XPS. The base pressure in the chamber was 1×10^{-10} mbar. In our studies, Al-Kα radiation was used. Details of the experimental procedures can be found in our previous report [29].

The sample total transmittances were recorded at room temperature with unpolarized light at normal incidence in the wavelength range from 300 nm to 1700 nm using a Cary 5000 (Varian) UV-Vis-NIR spectrophotometer equipped with an integrating sphere [29]. The reference was a FTO coated glass substrate cleaned exactly according to the same procedure as the substrates. Raman scattering was measured at room temperature with a Horiba Jobin Yvon LabRam IR system in a backscattering configuration. A 632.8 nm line of a He–Ne laser was used for off-resonance excitation with less than 4 mW power at the sample. The instrument was calibrated to the same accuracy using silicon and naphthalene standards. Photoluminescence (PL) was measured at 300 K and 10 K. The continuous wave (CW) photoluminescence (PL) was excited by the 4th harmonic (266 nm) of a Nd:YAG laser and dispersed with a HR250 monochromator (Jobin-Yvon) coupled to an UV-enhanced Intensified Charge Coupled Device (ICCD) (Roper). Under pulsed laser excitation, PL spectra were recorded in a pseudo CW mode with a continuous integration of the intensity in 300 ms corresponding to 3 full illumination pulses.

3. Results and discussion

X-ray diffraction was used to investigate the phase structure and lattice parameters of the ZnO:Eu nanowires. Results on pure ZnO nanowires grown by electrodeposition were presented previously [4,28]. Fig. 1 shows the X-ray diffraction pattern recorded in the 25–130° range with a scanning step of 0.02° of Eu(2.5 μM)-doped ZnO nanowires grown on F-SnO_2/glass substrate (sample #3). The pattern matches the lattice spacing of crystalline ZnO in the wurtzite structure (space group: $P6_3mc$(186)) [29].

All dot-marked (blue on-line) XRD peaks (Fig. 1) are assigned to FTO-coated glass substrates according to the Joint Committee on Powder Diffraction Standards (JCPDS) PDF 01-041-1445 card [30] and the rest to ZnO based on PDF 036-1451 [30]. Using a logarithmic scale, two tiny Eu_2O_3 diffraction peaks could be detected in this sample, whereas no Eu_2O_3 peaks were detectable for lower concentration of doping Eu(1.0 μM)-ZnO nanowires (not shown). It was detected for all electrodeposited ZnO nanowire arrays a sharp XRD reflection peak at ~34.43°, showing a preferential growth along the *c*-axis normal to the FTO substrate. By analyzing the

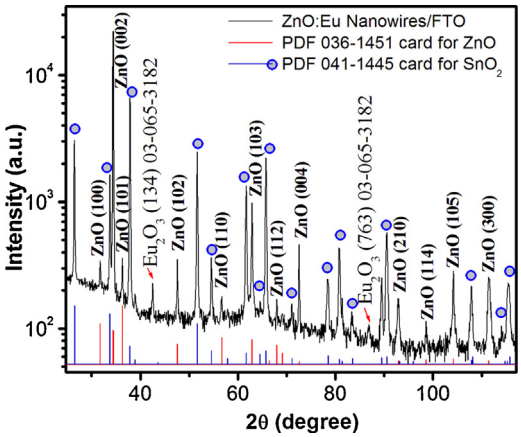

Fig. 1. X-ray diffraction pattern of Eu(2.5 μM)-doped ZnO nanowires grown by electrochemical method at 90 °C on FTO substrate. FTO substrate peaks are marked by blue dots and ZnO by red lines according to JCPDS. (For interpretation of the references to color in this figure legend, the reader is referred to the web version of the article.)

Table 1
Initial [Eu(III)] present in the electrolyte and final Eu-content in the ZnO:Eu nanowires as measured by EDX.

Sample	Initial [$EuCl_3$] in the starting aqueous electrolyte (μM)	Molar Eu content determine by EDX (%)[a]
#1	0	0.0
#2	1.0	1.2
#3	2.5	2.1

[a] Defined as the ratio [Eu]/[Eu+Zn].

logarithmic XRD pattern of Eu-ZnO nanowires, we found that, for dopings higher than 2.5 μM, the peaks at 42.45° and 86.86° attributable to cubic phase of Eu_2O_3 according to PDF 03-065-3182, increased in intensity. The high intensity of the ZnO peaks relative to the background clearly indicates good crystallinity of the samples. To confirm the possible substitution of Zn ions with Eu ions in ZnO:Eu NWs, the angle shift of 2θ for the ZnO (0 0 0 2) peak as a function of doping was observed. This shift increases up to 0.1° as doping rises from 0 to 2.5 μM, suggesting the substitution of Zn^{2+} by Eu cations in the crystalline NW lattice. Similar shifts were reported before [31,32]. The calculated Eu-doped ZnO lattice constants were determined according to [29,33]: $a = b = 3.2506$ Å, $c = 5.2055$ Å for pure ZnO NWs; $a = b = 3.2506$ Å, $c = 5.2076$ Å for ZnO:Eu (1 μM); $a = b = 3.2507$ Å, $c = 5.2096$ Å for ZnO:Eu (2.5 μM) nanowire arrays. It can be seen that compared to pure ZnO nanowires the *c*-lattice parameter progressively became slightly expanded by introducing a higher concentration of Eu ions into ZnO. According to our results, we can suggest that the solubility of Eu^{3+} ion into the ZnO lattice is limited to about 2.5 μM in solution in case of ECD. These results are in agreement with previous observations of limited Eu solubility in the ZnO matrix [25,31,6,34,32].

Fig. 2a and 2b are top- and lateral-views of ZnO:Eu (2.5 μM) nanowire arrays grown on FTO substrates at 90 °C for 9000 s. Based on these SEM images, it can be concluded that sample ECD at 90 °C has a high-aspect ratio in good agreement with previous report on pure ZnO by Pauporté et al. [35]. The mean nanowire diameter was about 125 nm and the length was about 2200 nm. The wires in Fig. 2b have well-defined edges. Analysis by energy dispersive X-ray spectroscopy (EDX) have been done to estimate the molar Eu content in the nanowire arrays prepared in the presence of europium chloride on FTO substrate. The results are reported in Table 1. The molar ratio between europium and zinc in the ZnO NWs increased with the europium content in the bath and was significantly lower than that in the deposition bath. The [Eu]/[Zn+Eu] molar content in zinc oxide nanowires was found about 1.2% and 2.1% for samples #2 and #3, respectively.

TEM and selected electron diffraction (SAED) were employed to gain insight into the structure of an individual nanowire with uniform diameter in sample #3 and the results are presented in Fig. 3. We can clearly see that the NWs had a uniform diameter along their length (Fig. 3a). The corresponding high-resolution TEM image taken from the edge of the sample reveals the ZnO {0 0 0 1} planes of the hexagonal ZnO in Fig. 3b. The interplanar spacing of 0.52 nm matches well with the (0 0 0 1) plane of wurtzite ZnO, indicating that the nanowire is single crystalline and grows along the $\langle 0\,0\,0\,1 \rangle$ direction (*c*-axis being the preferential growth). The associated SAED pattern indicates that the ZnO:Eu-nanowires have a single crystal structure and do not display any noticeable defects in the investigated areas. Fig. 3c shows that the growth direction was the $\langle 0\,0\,0\,1 \rangle$ *c*-axis. The chemical composition of the pure and Eu-doped ZnO nanowires was investigated by SIMS. Fig. 4 shows Zn, Eu and Sn signals from sample #3 versus the sputtering time. The Eu count rate seems to closely follow the Zn count rate over most of the sample depth. This is an indication that the Eu dopant was quite homogeneously incorporated throughout the ZnO nanowire

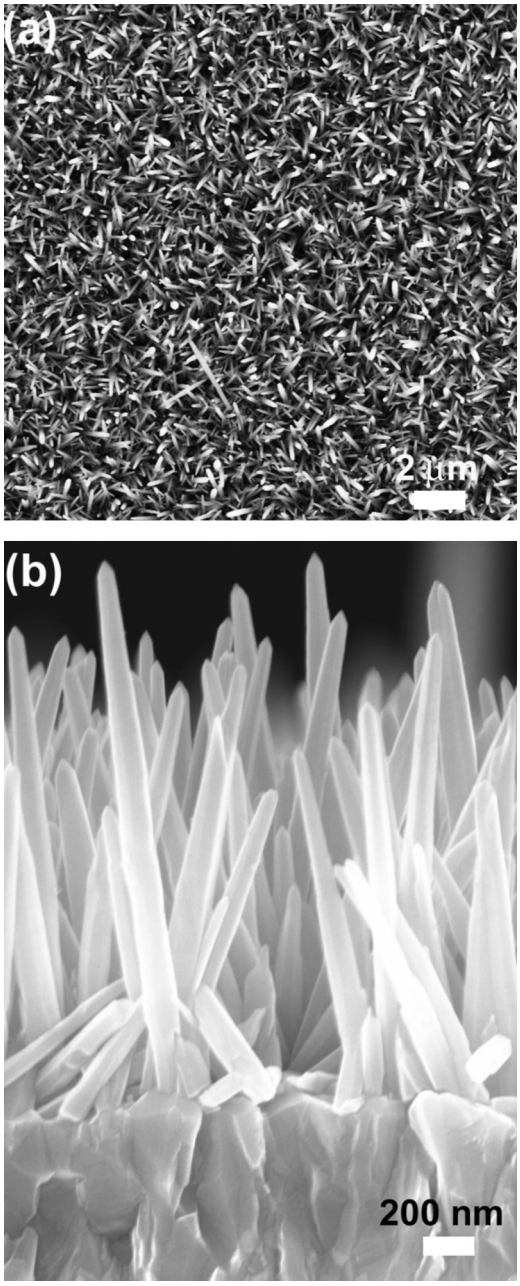

Fig. 2. SEM micrographs of a sample #3 nanowire arrayed layer electrodeposited on FTO substrate at 90 °C for 9000 s: (a) top-view and (b) lateral-view.

structure. As expected, no correlation between the Eu and Sn (from the FTO substrate) count rates was observed, and a gradual increase in the Sn signal until saturation was observed as a function of the sputtering time.

To further illuminate the detailed chemical composition of the nanowires, XPS was used to characterize the composition of sample #2 and sample #3. XPS data of pure ZnO NWs were include in Ref. [33,36]. Positive binding energy (BE) shifts were observed in the XPS spectra due to charging effects. Therefore, the BE scale was calibrated using the adventitious carbon peak (C-1s) at 285 eV as reference. In our samples, residual amounts of adventitious carbon and carbonyl compounds were unavoidable due to their exposure to air prior to the XPS analysis [36]. Fig. 5a shows XPS spectra of the Zn-2p core level region. The Eu-doped ZnO nanowires display a doublet at 1021.9 eV and 1045 eV (vertical reference lines) corresponding to the Zn-$2p_{3/2}$ and $2p_{1/2}$ core levels, respectively

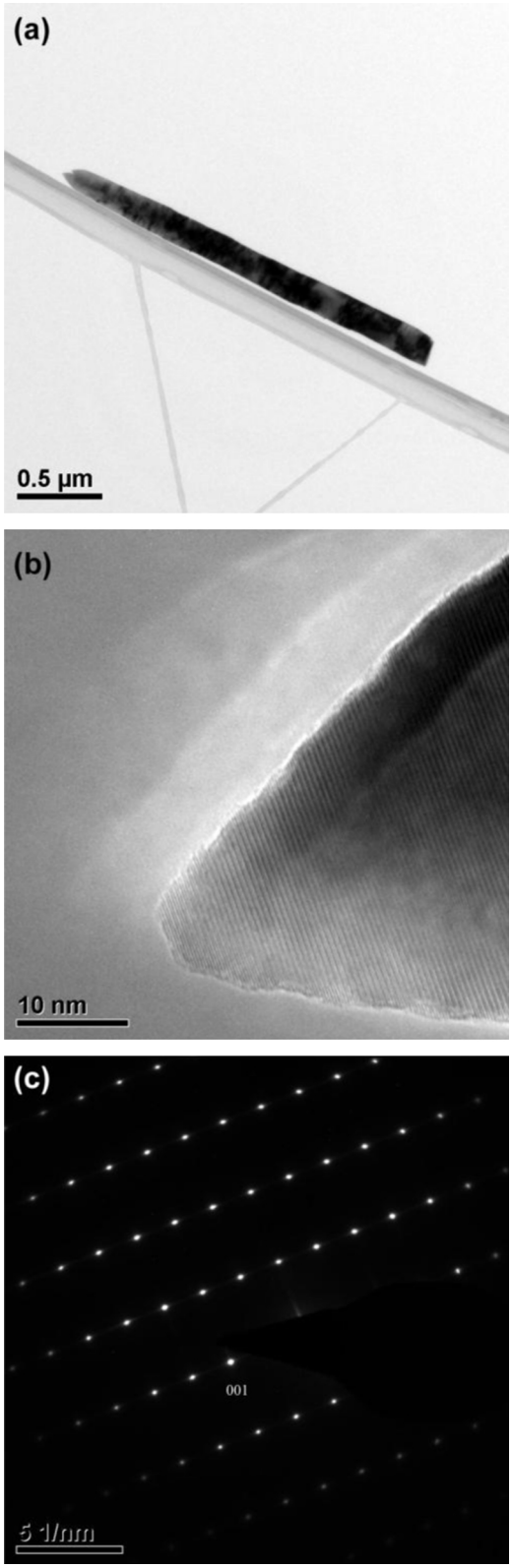

Fig. 3. (a) TEM image of the sample #3-nanowire on carbon holey TEM grid revealing the surface morphology along the entire nanowire. (b) HRTEM image of the ZnO:Eu nanowire tip. (c) Selected area electron diffraction (SAED) pattern of the sample.

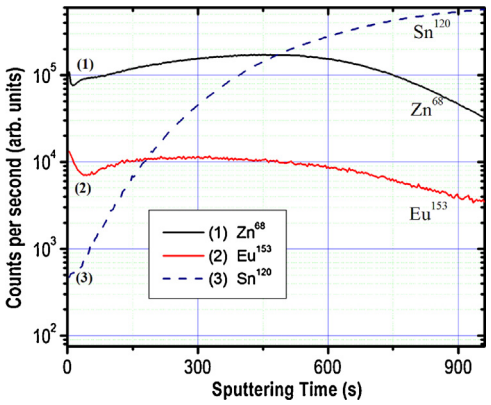

Fig. 4. SIMS measurements of sample #3. The dashed curve (Sn) corresponds to the FTO substrate.

[37]. The asymmetric feature observed in the O-1s region, Fig. 5b, was deconvoluted by two subspectral components: stoichiometric ZnO (530.5 eV), and defective ZnO_x (531.8 eV) [38]. Based on the O-1s XPS data, the relative contents of ZnO and ZnO_x species were 61% and 39%, respectively, and very similar in both Eu-doped samples.

The Eu-3d XPS BE region of the Eu-doped ZnO nanorod samples is shown in Fig. 6. This BE region could be fitted with two doublets assigned to the Eu-$3d_{5/2}$ and $3d_{3/2}$ core levels of two different species: (i) Eu^{2+}-$3d_{5/2}$ (Eu-$3d_{5/2}$ = 1126 eV, 26% of the total Eu XPS signal) and (ii) Eu^{3+}-$3d_{5/2}$ (Eu-$3d_{5/2}$ = 1135.4 eV, 74%) [39,40]. The fact that only cationic Eu species were detected in these samples suggests the incorporation of Eu into the ZnO matrix, as reported by Du et al. [41] for ZnO nanocrystals.

The optical total transmission spectra of Eu-doped ZnO NW samples are shown in Fig. 7. Sample #2 and sample #3 have a transmittance higher than 70% in the visible region and higher than 90% in the near-infrared one. Pure ZnO NWs show a transmittance higher than 62% in the visible region and it is higher than 90% in the near-infrared range. The interference fringes are due to the superposition of waves that originate from the same point of the same source. The interference fringes most likely are due to the FTO film on the glass substrates. Raman spectroscopy is recognized as a powerful technique for the characterization of nanocrystal structures. To see dopant influence on the Raman scattering and to obtain more information on the microstructure of ECD ZnO:Eu NWs with two different concentrations of $EuCl_3$ in the bath, their room-temperature Raman spectra were analyzed. ZnO belongs to the wurtzite space group C_{6v}^4 and phonon modes E_2 (low and high frequency), A_1 [(TO)-transverse optical and (LO)-longitudinal optical] and E_1 (TO and LO) are expected all being Raman and infrared active, B_1 mode keeps silence. The optical phonons at the Γ point of the Brillouin zone belong to the representation [29]:

$$\Gamma_{\text{opt}} = 1A_1 + 2B_1 + 1E_1 + 2E_2 \quad (1)$$

Fig. 8 shows the Raman spectra measured in backscattering geometry in the annealed ZnO:Eu nanowire arrays ECD on FTO substrate. The Raman emissions from the FTO layer presents broad peaks at 106, 122, 244, 284, 373, 472, 494, 561, 633 cm^{-1} [29] and can be found in all spectra of our samples. The E_2(low) (100 cm^{-1}) mode in ZnO is associated with the vibration of heavy Zn sub-lattice and the E_2(high) mode involves only the oxygen atoms. The Raman peak at 436 cm^{-1} is assigned to the ZnO nonpolar optical phonons of high-E_2 mode, which is one of the characteristic peaks of wurtzite ZnO [29]. The band at 327 cm^{-1} is attributed to the overtone of A_1. The main Raman peak at 436 cm^{-1} E_2-high clearly shifts toward lower wavenumber as Eu-concentration increases confirming an effective substitution of Zn^{2+} by Eu^{3+} (Eu^{2+}) ions in the investigated samples [13,42–48], in agreement with XRD, SIMS and XPS results.

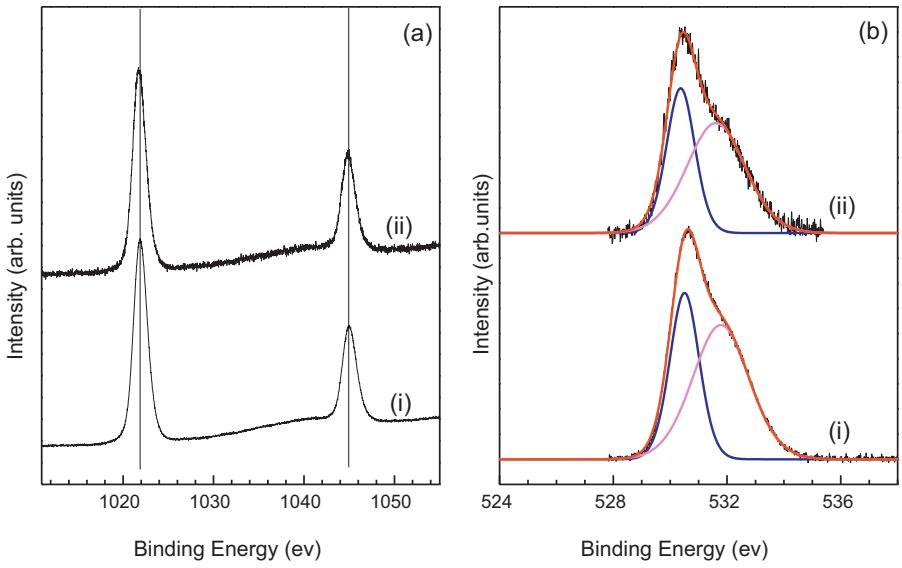

Fig. 5. XPS spectra (Al Kα = 1486.6 eV) corresponding to the (a) Zn-2p and (b) O-1s core level regions of (i) sample #2 and (ii) sample #3.

It can also be observed, a peak broadening caused by a phonon confinement effect [49–52]. Moreover, as the Eu concentration in bath increases from 1.0 μM to 2.5 μM and above, the Raman line E_2(high) mode becomes broadened, which means that the crystallinity of ZnO decreases [49,50]. The relatively small shift suggests small stress in the ZnO:Eu NWs, which can be attributed to the stress relaxation effect in the nanorods [8,53–55]. It is of importance to mention that signals corresponding to any other europium species in the Raman spectra were not detected. This demonstrates that the doped nanowires keep the same wurtzite structure as ZnO when there are no apparent detectable impurities as reported before [41].

The optical quality and the emission properties of the electrodeposited ZnO:Eu NW arrays were characterized by photoluminescence (PL) measurements. Fig. 9a shows the photoluminescence (PL) of sample #3 recorded under UV excitation at 266 nm using the fourth harmonic of YAG:Nd laser. The emission peak centered at 382 nm is characteristic of ZnO near band edge recombination. By using a logarithmic scale, a weak green luminescence due to ZnO intrinsic defects was observed at about 530 nm whereas no red emission due to the Eu dopant could be detected [8,53]. The samples were also investigated using intensified CCD detector and pumping at 394 nm in the 4f–4f Eu^{3+} absorption band with a pulse delay of 100 ns to prevent the detection of the band to band UV recombination. Fig. 9b shows a magnified broad emission at 530 nm for samples #2 and #3 which can be assigned to defects in ZnO or possibly to the 5d–4f Eu^{2+}

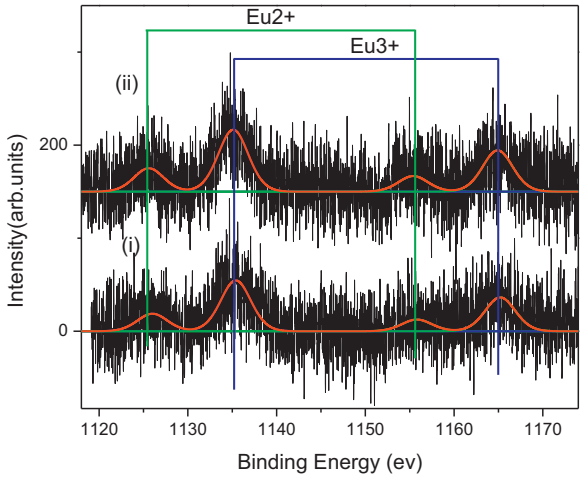

Fig. 6. XPS spectra (Al Kα = 1486.6 eV) corresponding to the Eu-3d core level region of (i) sample #2 and (ii) sample #3.

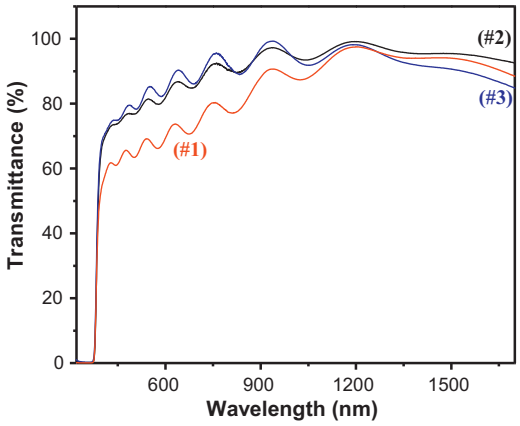

Fig. 7. Optical total transmission curves of the three samples: pure ZnO, sample #1 and ZnO:Eu NWs ECD with two different concentrations of $EuCl_3$ in the bath, sample #2 and sample #3.

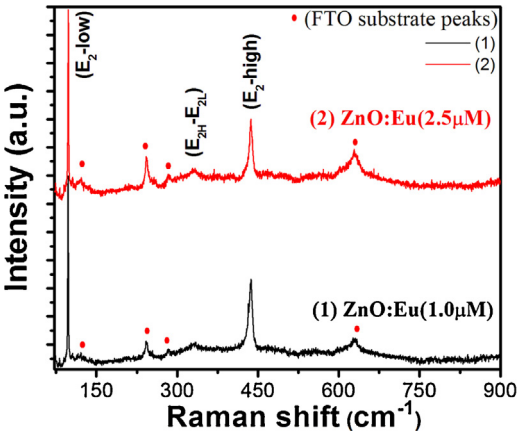

Fig. 8. Raman spectra of NWs ECD with two different concentrations of $EuCl_3$ in the bath: (1) sample #2 and (2) sample #3.

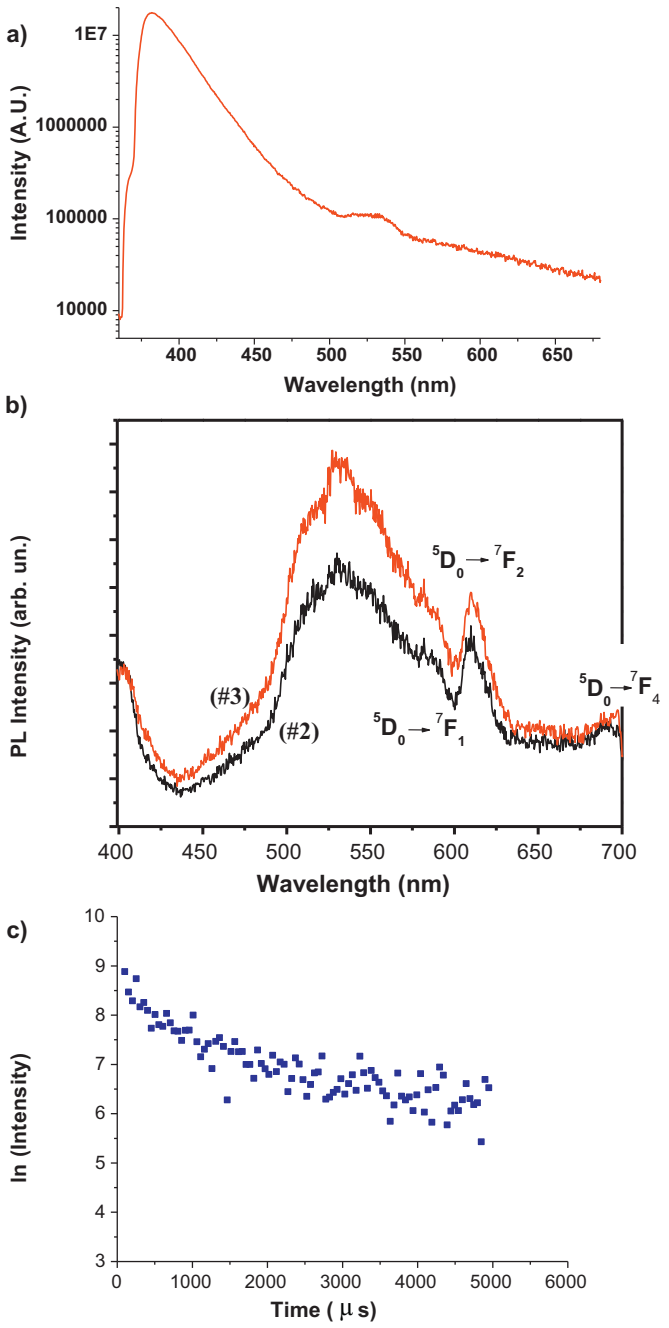

Fig. 9. (a) Room temperature logarithmic scaled PL spectrum of sample #3 under excitation at 266 nm. (b) Visible emission spectrum at 10 K under pumping at 394 nm (samples #2 and #3) and (c) time decay profile for the 612 nm emission of sample #3 measured in (b).

emission. On the other hand, the narrow peak at around 612 nm and satellite emissions can be attributed to the Eu^{3+} ions ($^5D_0 \rightarrow {}^7F_2$ transition for the strongest one). At 394 nm, direct resonant excitation occurs in the $^7F_0$–^5F_j transitions of Eu^{3+} ions in ZnO nanowires. The $^5D_0 \rightarrow {}^7F_2$ transition lifetime at 10 K (Fig. 9c), was measured at about 1.7 ms for the first part of the decay and is characteristic of a Eu^{3+} transition. The non-exponential profile probably indicates energy transfer between europium species. Furthermore, we have observed that the emission at 612 nm (Eu^{3+}) vanished when the temperature was increases (not shown). The presence of two oxidation europium states, demonstrated by XPS measurements, and defects could give rise to non-radiative energy transfers preventing the efficient europium emission.

4. Conclusions

We have shown that dense arrays of Eu-doped ZnO nanowires can be prepared by an original electrochemical technique and that their Eu content can be adjusted by varying the $EuCl_3$ precursor concentration in the deposition bath. The synthesis procedure is simple, reproducible and low-cost since it does not require expensive equipment. The synthesis is done at low temperature and at atmospheric pressure. The substitution of Zn by Eu in the crystal lattice has been shown by XRD measurements. Eu doping was quite uniform along the nanowires. High-resolution TEM studies indicated a <0001> growth direction along the *c*-axis of the hexagonal ZnO and the associated selected electron diffraction showed the single crystal structure without noticeable defects in the ZnO:Eu nanowires. According to SIMS and XPS studies, only cationic Eu species were detected suggesting the incorporation of Eu into the ZnO lattice. The valence state of europium ions in the nanowires was determined as predominately +3. Direct resonant excitation of Eu in the material led to the sharp red emission at around 612 nm due to $^5D_0$–$^7F_2$ transition of the Eu^{3+} ion. These results suggest that Eu-doped ZnO nanowires could pave the way for efficient, multispectral LEDs and optical devices.

Acknowledgements

Dr. O. Lupan acknowledges the CNRS for support as an invited scientist at the LECIME-LCMCP and financial support of the STCU and ASM through grant 09STCUA/5833. B.R.C. gratefully acknowledges the financial aids from the NSF-DMR-0906562. This research was performed with the financial support of the C-nano Ile-de-France DIM program (Effi-NanoLED Project).

References

[1] O. Lupan, T. Pauporté, B. Viana, Advanced Materials 22 (2010) 3298–3302.
[2] S. Xu, C. Xu, Y. Liu, Y. Hu, R. Yang, Q. Yang, J.-H. Ryou, H.J. Kim, Z. Lochner, S. Choi, R. Dupuis, Z.L. Wang, Advanced Materials 22 (42) (2010) 4749–4753.
[3] O. Lupan, T. Pauporté, T. Le Bahers, B. Viana, I. Ciofini, Advanced Functional Materials 21 (2011) 3564–3572.
[4] O. Lupan, T. Pauporté, B. Viana, P. Aschehoug, Electrochimica Acta 56 (2011) 10543–10549.
[5] P. Mukherjee, C.M. Shade, A.M. Yingling, D.N. Lamont, D.H. Waldeck, S. Petoud, Journal of Physical Chemistry A 115 (2011) 4031–4041.
[6] A. Ishizumi, Y. Kanemitsu, Applied Physics Letters 86 (2005) 253106.
[7] T.V. Butkhuzi, T.G. Chelidze, A.N. Georgobiani, D.L. Jashiashvili, T.G. Khulordava, B.E. Tsekvava, Physical Review B 58 (1998) 10692.
[8] S.T. Shishiyanu, O.I. Lupan, E.V. Monaico, V.V. Ursaki, T.S. Shishiyanu, I.M. Tiginyanu, Thin Solid Films 488 (2005) 15–19.
[9] M.D. McCluskey, S.J. Jokela, Journal of Applied Physics 106 (2009) 071101.
[10] X. Zeng, J. Yuan, Z. Wang, L. Zhang, Advanced Materials 19 (2007) 4510–4514.
[11] T. Pauporté, F. Pellé, B. Viana, P. Aschehoug, Journal of Physical Chemistry C 111 (2007) 15427–15432.
[12] A. Goux, T. Pauporté, D. Lincot, Electrochimica Acta 53 (2007) 50–58.
[13] Y.P. Du, Y.W. Zhang, L.D. Sun, C.H. Yan, Journal of Physical Chemistry C 112 (2008) 12234–12241.
[14] Y. Yu, Y. Wang, D. Chen, P. Huang, E. Ma, F. Bao, Nanotechnology 19 (2008) 055711.
[15] Y.H. Yang, Y. Feng, H.G. Zhu, G.W. Yang, Journal of Applied Physics 107 (2010) 053502.
[16] K. Ebisawa, T. Okuno, K. Abe, Japanese Journal of Applied Physics 47 (2008) 7236–7238.
[17] R. Chen, Y.Q. Shen, F. Xiao, B. Liu, G.G. Gurzadyan, Z.L. Dong, X.W. Sun, H.D. Sun, Journal of Physical Chemistry C 114 (2010) 18081–18084.
[18] D. Wang, G. Xing, M. Gao, L. Yang, J. Yang, T. Wu, Journal of Physical Chemistry C 115 (2011) 22729–22735.
[19] C.J. Pan, C.W. Chen, J.Y. Chen, P.J. Huang, G.C. Chi, C.Y. Chang, F. Ren, S.J. Pearton, Applied Surface Science 256 (2009) 187–190.
[20] S.K. Lathika Devi, K. Sudarsana Kumar, A. Balakrishnan, Materials Letters 65 (2011) 35–37.
[21] P. Mohantya, B. Kima, J. Park, Materials Science and Engineering B 138 (2007) 224–227.
[22] I.W. Lenggoro, Y. Itoh, K.J. Okuyama, Materials Research 19 (2004) 3534.
[23] C. Panatarani, I.W. Lenggoro, K.J. Okuyama, Physics and Chemistry of Solids 65 (2004) 1843.
[24] W. Jia, K. Monge, W. Xu, R. Katiyar, Integrated Ferroelectrics 42 (2002) 357.

[25] A. Ishizumi, Y. Taguchi, A. Yamamoto, Y. Kanemitsu, Thin Solid Films 486 (2005) 50.
[26] Z. Shen, P.E. Burrows, V. Bulovic, S.R. Forrest, M.E. Thompson, Science 276 (1997) 2009.
[27] A. Goux, T. Pauporté, D. Lincot, Electrochimica Acta 51 (2006) 3168.
[28] B. Viana, O. Lupan, T. Pauporte, Journal of Nanophotonics 5 (2011) 051816.
[29] O. Lupan, T. Pauporté, L. Chow, B. Viana, F. Pelé, L.K. Ono, B. Roldan Cuenya, H. Heinrich, Applied Surface Science 256 (2010) 1895.
[30] American Society for Testing and Material, Powder Diffraction Files, Joint Committee on Powder Diffraction Standards, Swarthmore, PA, 1996, pp. 3–888.
[31] Y.-P. Du, Y.-W. Zhang, L.-D. Sun, C.-H. Yan, Journal of Physical Chemistry C 112 (2008) 12234–12241.
[32] C.C. Yang, S.Y. Cheng, H.Y. Lee, S.Y. Chen, Ceramics International 32 (2006) 37.
[33] O. Lupan, T. Pauporté, I.M. Tiginyanu, V.V. Ursaki, V. Şontea, L.K. Ono, B. Roldan Cuenya, L. Chow, Thin Solid Films 519 (2011) 7738–7749.
[34] S.A.M. Lima, F.A. Sigoli, M.R. Davolos, M. Jafelicci, Journal of Alloys and Compounds 344 (2002) 280.
[35] T. Pauporté, E. Jouanno, F. Pellé, B. Viana, P. Aschehoug, Journal of Physical Chemistry C 113 (2009) 10422–10431.
[36] O. Lupan, T. Pauporté, Le T. Bahers, I. Ciofini, B. Viana, Journal of Physical Chemistry C 115 (30) (2011) 14548.
[37] O. Lupan, G. Emelchenko, V.V. Ursaki, G. Chai, N. Redkin, N. Gruzintsev, I.M. Tiginyanu, L. Chow, L.K. Ono, B. Roldan Cuenya, H. Heinrich, E.E. Yakimov, Materials Research Bulletin 45 (2010) 1026–1032.
[38] J. Liqiang, W. Dejun, W. Baiqi, L. Shudan, X. Baifu, F. Honggang, S. Jiazhong, Journal of Molecular Catalysis A 244 (2006) 193–200.
[39] O. Lupan, L. Chow, L.K. Ono, B. Roldan Cuenya, G. Chai, H. Khallaf, S. Park, A. Schulte, Journal of Physical Chemistry C 114 (2010) 12401–12408.
[40] J. Zhang, M. Zhou, B. Liu, Y. Wen, Y. Wang, Journal of Luminescence 132 (2012) 1949–1952.
[41] J. Qi, T. Matsumoto, M. Tanaka, Y. Masumoto, Journal of Physics D: Applied Physics 33 (2000) 2074.
[42] J. Rousset, E. Saucedo, D. Lincot, Chemistry of Materials 21 (2009) 534–540.
[43] J. Hamberg, C.G. Granqvist, Journal of Applied Physics 60 (1986) R123.
[44] X.L. Wu, G.G. Siu, C.L. Fu, H.C. Ong, Applied Physics Letters 78 (2001) 2285.
[45] N. Jaba, A. Mermet, E. Duval, B. Champagnon, Journal of Non-Crystalline Solids 351 (2005) 833.
[46] K. Samanta, P. Bhattacharya, R.S. Katiyar, Physical Review B 73 (2006) 245213.
[47] K. Samanta, S. Dussan, R.S. Katiyara, P. Bhattacharya, Applied Physics Letters 90 (2007) 261903.
[48] X.F. Wang, J.B. Xu, X.J. Yu, K. Xue, J.G. Yu, X. Zhao, J. Applied Physics Letters 91 (2007) 031908.
[49] T. Pauporté, O. Lupan, B. Viana, Physica Status Solidi A 209 (2012) 359–363.
[50] H. Richter, Z.P. Wang, L. Ley, Solid State Communications 39 (1981) 625.
[51] G. Viera, S. Huet, L. Boufendi, Applied Physics Journal 90 (2001) 4175.
[52] F. Wang, H. He, Z. Ye, L. Zhu, H. Tang, Y. Zhang, Journal of Physics D: Applied Physics 38 (2005) 2919–2922.
[53] O. Lupan, T. Pauporté, V.V. Ursaki, I.M. Tiginyanu, Optical Materials 33 (2011) 914–919.
[54] O. Lupan, T. Pauporté, B. Viana, V.V. Ursaki, I.M. Tiginyanu, V. Sontea, L. Chow, Journal of Nanoelectronics and Optoelectronics 7 (2012) 712–718.
[55] O. Lupan, L. Chow, Th. Pauporté, L.K. Ono, B. Roldan Cuenya, G. Chai, Sensor. Actuat. B- Chem. 173 (2012) 772–780.